Modelling the impact of nucleolin expression level on the activity of F3 peptide-targeted pH-sensitive pegylated liposomes containing doxorubicin

As Published: https://doi.org/10.1007/s13346-021-00972-z

Publisher: Springer US

Persistent URL: https://hdl.handle.net/1721.1/139779

Version: Author's final manuscript: final author's manuscript post peer review, without publisher's formatting or copy editing

Modelling the impact of nucleolin expression level on the activity of F3 peptide-targeted pH-sensitive pegylated liposomes containing doxorubicin

Cite this article as: Rui Lopes, Kevin Shi, NunoA. Fonseca, Adelina Gama, JoséS. Ramalho, Luís Almeida, Vera Moura, Sérgio Simões, Bruce Tidor, JoãoN Moreira, Modelling the impact of nucleolin expression level on the activity of F3 peptide-targeted pH-sensitive pegylated liposomes containing doxorubicin, Drug Delivery and Translational Research https://doi.org/10.1007/s13346-021-00972-z

Modelling the impact of nucleolin expression level on the activity of F3 peptide-targeted pH sensitive pegylated liposomes containing doxorubicin

Lopes, Rui[a*]; Shi, Kevin[b*]; Fonseca, Nuno A.[a,c*]; Gama, Adelina[c]; Ramalho, José S.[d]; Almeida, Luís[e]; Moura, Vera[c]; Simões, Sérgio[a,f]; Tidor, Bruce[b,**], Moreira, João N[a,f,**]

[a] CNC – Center for Neurosciences and Cell Biology, Center for Innovative Biomedicine and Biotechnology (CIBB), University of Coimbra, Faculty of Medicine (Polo 1), Rua Larga, 3004-504 Coimbra, Portugal

[b] Department of Biological Engineering and Department of Electrical Engineering and Computer Science, Massachusetts Institute of Technology, Cambridge, MA, 02139, USA

[c] TREAT U, SA - Parque Industrial de Taveiro, Lote 44, 3045-508 Coimbra, Portugal

[c] Animal and Veterinary Research Centre (CECAV), University of Trás-os-Montes and Alto Douro (UTAD), Quinta de Prados, Apartado 1013, 5000-801, Vila Real, Portugal

[d] Laboratory of Cellular and Molecular Biology, NOVA Medical School, New University of Lisbon, Campo Mártires da Pátria, 130, 1169-056 Lisboa Portugal

[e] Blueclinical, Ltd, 4460-439 Senhora da Hora, Matosinhos, Portugal

[f] UC – University of Coimbra, CIBB, Faculty of Pharmacy, Pólo das Ciências da Saúde, Azinhaga de Santa Comba, 3000-548 Coimbra, Portugal

* These authors contributed equally.

** Corresponding authors: jmoreira@ff.uc.pt; tidor@mit.edu.

Abstract

Strategies targeting nucleolin have enabled a significant improvement in intracellular bioavailability of their encapsulated payloads. In this respect, assessment of the impact of target cell heterogeneity and nucleolin homology across species (structurally and functionally) is of major importance. This work also aimed at mathematically modelling the nucleolin expression levels at the cell membrane, binding and internalization of pH-sensitive pegylated liposomes encapsulating doxorubicin and functionalized with the nucleolin-binding F3 peptide (PEGASEMP), and resulting cytotoxicity against cancer cells from mouse, rat, canine and human origin.

Herein it was shown that nucleolin expression levels were not a limitation on the continuous internalization of F3 peptide-targeted liposomes, despite the saturable nature of the binding mechanism. Modeling, enabled the prediction of nucleolin-mediated total doxorubicin exposure provided by the experimental settings of the assessment of PEGASEMP's impact on cell death. The former increased proportionally with nucleolin-binding sites, a measure relevant for patient stratification. This pattern of variation was observed for the resulting cell death in non-saturating conditions, depending on the cancer cell sensitivity to doxorubicin. This approach differs from standard determination of cytotoxic concentrations, which normally report values of incubation doses rather than the actual intracellular bioactive drug exposure. Importantly, in the context of development of nucleolin-based targeted drug delivery, the structural nucleolin homology (higher than 84%) and functional similarity across species presented herein, emphasized the potential to use toxicological data and other metrics from lower species to infer the dose for a first-in-human trial.

Graphical Abstract

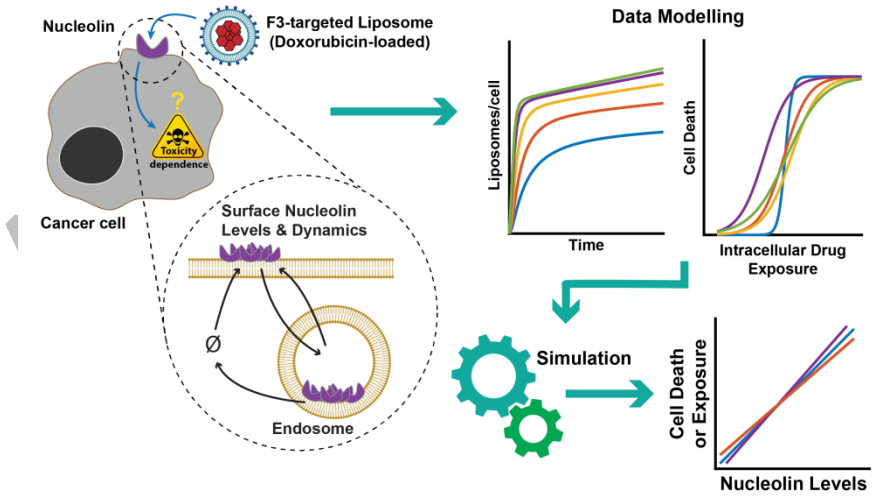

Key-Words

Nanomedicine; Ligand-mediated targeting; Nucleolin expression; Modelling; Protein homology.

Introduction

Liposomal doxorubicin demonstrates an improved safety profile over conventional free doxorubicin in patients [1]. However, those with breast or ovarian cancer did not benefit from improved efficacy relative to free doxorubicin, in contrast with preclinical data. These results demonstrate the need to engineer alternative mechanisms that go beyond classical EPR (Enhanced Permeability and Retention) effect-driven accumulation in solid tumors [2]. By exploring the receptor-ligand interaction mechanism, significant advances in efficacy may be achieved from improvement of associated drug bioavailability at the tumor site and/or accumulation of ligand-mediated targeted nanoparticle [3]. To this end, various nanotechnology-based targeting strategies have been explored at the pre-clinical level. A large body of work on the characterization of target receptor-nanoparticle interactions has been generated for HER2 antibody-targeted liposomal doxorubicin (MM-302, from Merrimack Pharmaceuticals). These studies aimed at gaining a better understanding of which tumors would be most susceptible to treatment and with which non-target tissues putative interactions would occur [4]. Additionally, the receptor HER2 has also been explored at the clinical level [5].

Nucleolin is being explored as a novel target for different innovative therapeutic strategies [6, 7]. Nucleolin is a nucleolar protein involved in various cellular functions that control nucleic acid metabolism, cell cycle, microtubule nucleation and nucleolus structure [8-10]. Its overexpression has been identified in several neoplasias, suggesting its role as an unfavorable prognostic factor [11-15]. In fact, under pathological conditions, it can drive tumorigenesis by promoting invasion and angiogenesis [16]. Furthermore, the increased localization of nucleolin in the cell membrane, in both cancer cells and the endothelial cells of tumor angiogenic blood vessels, modulates the internalization of different ligands and nucleus-cytoplasm-membrane shuttling [17-19].

Different drug delivery strategies targeting nucleolin have actually benefited from this mechanism, as it enables a significant improvement in intracellular bioavailability of their encapsulated payloads [2, 7, 18]. Thus, characterizing and modelling the interactions between nucleolin and a nucleolin-binding nanoparticle, such as via the F3 peptide [17, 20], across cancer cells of different species with different surface nucleolin expression levels, is of major importance. This will enable better assessments of the impact of target cell heterogeneity and nucleolin homology across species (structurally and functionally). Such an approach, and modelling in particular, may also enable the optimization of patient stratification, with translation into efficacy and safety gains, while providing information for clinical development decisions [4].

Accordingly, the objective of this work was to characterize and mathematically model the interaction between nucleolin expression levels at the cell membrane, binding and internalization of pH-sensitive

pegylated liposomes encapsulating doxorubicin and functionalized with the nucleolin-binding F3 peptide (PEGASEMP) [7] and resulting cytotoxicity against breast cancer cells from mouse, canine and human origin. Nucleolin trafficking, liposome binding, and drug distribution mechanisms have all been modeled as systems of nonlinear ordinary differential equations as previously described [21]. A single model was developed to capture the behavior in the different cancer cell lines with adjusted parameterizations depending on the species and the particular cell line. This enabled direct comparisons between cell line behaviors, including at a foundational mechanistic level. Altogether, it was possible to probe the relation between nucleolin cell surface density to cellular association, internalization, and cell killing of liposomes targeted by the nucleolin-binding F3 peptide in cancer cells from diverse species.

Material and Methods

Materials

4-(2-hydroxyethyl)piperazine-1-ethanesulfonic acid (HEPES), 2-(N-morpholino)ethanesulfonic acid (MES), disodium ethylenediaminetetraacetate dehydrate (EDTA), sodium chloride, 3β-hydroxy-5-cholestene-3-hemisuccinate (CHEMS) and cholesterol (CHOL) were purchased from Sigma-Aldrich (USA). The lipids 2-dioleoyl-sn-glycero-3-phosphoethanolamine (DOPE), 1,2-distearoyl-sn-glycero-3-phosphocholine (DSPC), 1,2-distearoyl-sn-glycero-3-phosphoethanolamine-N-[methoxy(polyethylene glycol)-2000] (DSPE-PEG_{2k}), 1,2-distearoyl-sn-glycero-3-phosphoethanolamine-N-[maleimide(polyethylene glycol)-2000] (DSPE-PEG_{2k}maleimide) and 1,2-dioleoyl-sn-glycero-3-phosphoethanolamine-N-(lissamine rhodamine B sulfonyl) (Rho-PE) were obtained from Avanti Polar Lipids (USA). DSPE-PEG_{2k}-F3 was costum synthesized as previously described [7]. F3 peptide and non-specific peptide (ARALPSQRSR) were custom synthetized by Genecust (Luxemburg). All other chemicals were of analytical grade purity. Anti-NCL-Alexa®488 antibody [mouse 364-5 clone, lot: GR149756-1] and IgG_{1k} isotype control were from Abcam (UK) and Affymetrix (USA), respectively. Quantum™ MESF Alexa488-labeled microsphere kit (lot: 1148 was acquired form Bangs Laboratories (USA).

Cell lines and cell culture

Several breast cancer cell lines of different animal origin were used, namely, 4T1 (mouse), MDA-MB-231 (ATCC) and CMT3 (canine). CMT3 cells were kindly provided by Adelina Gama, from the Animal and Veterinary Research Centre (CECAV), University of Trás-os-Montes and Alto Douro (UTAD), Vila Real, Portugal. Even though reclassified [22, 23], MDA-MB-435S cells (human) (ATCC) are an essential positive control to the study of ligands targeting nucleolin, as the case of the F3 peptide [17]. All cell lines were cultured in RPMI 1640 (Sigma-Aldrich, USA) supplemented with

10% (v/v) of heat-inactivated fetal bovine serum (FBS) (Invitrogen, USA), 100 U/ml penicillin, 100 µg/ml streptomycin (Lonza, Switzerland) and maintained at 37°C in a 5% CO_2 atmosphere.

Liposome preparation

Rhodamine-labeled pH-sensitive liposomes were prepared by the ethanol injection method as described previously [24]. Briefly, a lipid mixture DOPE:CHEMS:DSPC:CHOL:DSPE-PEG2k (4:2:2:2:0.18:0.12 molar ratio) and rhodamine-PE (1 mol% relative to total lipid) in absolute ethanol was dispersed into HBS buffer (25 mM HEPES, 140 mM NaCl, pH 7.4) previously heated at 65°C. The resulting liposomes were extruded 21 times through 50 nm pore size polycarbonate membranes using a LiposoFast Basic mini extruder (Avestin, Canada). The ethanol excess was removed by gel chromatography in a Sephadex G-50 gel column (Sigma-Aldrich, USA) equilibrated with HBS pH 7.4. To further prepare targeted liposomes, micelles of DSPE–PEG_{2k}–peptide conjugates were post-inserted onto the liposomal membrane at 2 mol% relative to total lipid, upon incubation with pre-formed liposomes, for 1 h at 50 °C. In respect to the non-targeted counterpart, post-insertion was performed only with plain DSPE-PEG micelles.

Liposome mean size and polydispersion index (PDI) were measured by light scattering with a N5 particle size analyzer (Beckman Coulter, USA). Final total lipid concentrations were determined upon quantification of cholesterol using the Liebermann–Burchard method [25]. Absorbance was measured at 625 nm in a spectrophotometer and the cholesterol content was determined from a standard curve.

F3 peptide-targeted pH-sensitive liposomal doxorubicin (codenamed PEGASEMP, 3 L pilot batch) was manufactured by ethanol injection method (similar as above) at Evonik Canada (formerly Northern Lipids, Canada) under Good Manufacturing Practices [7]. Resulting multilamellar vesicles were extruded through 80 nm membranes to form large unilamellar vesicles (LUVs). Encapsulation of doxorubicin was performed through remote loading [26]. Sterile filtration was performed before vial filling [7]. Typical characterization of these liposomes is described elsewhere [7, 24, 26, 27].

***In vitro* determination of cell surface nucleolin density by flow cytometry**

Determination of steady state surface levels of nucleolin is important to anticipate the activity of F3 peptide-targeted liposomes. Accordingly, from 80-90% confluent cell cultures, $2.5x10^5$ 4T1 (mouse), MDA-MB-231 and MDA-MB-435 (human) and CMT3 (canine), in RPMI 1640 supplemented with 10% (v/v) of heat-inactivated FBS, 100 U/mL penicillin, 100 µg/mL streptomycin, were transferred into Eppendorf tubes and placed on ice for 20-30 min. Following 3 min centrifugation (170 *g*), cells were then resuspended in 200 µL of cold PBS (phosphate buffer saline, pH 7.4) with 1% bovine serum albumin (PBS-BSA) and maintained on ice for 15-20 min. Cells were further centrifuged for

3 min at 170 g, resuspended in 100 µL of PBS-BSA containing 16.7 µM of DSPE-PEG_{2k}-F3 micelles and 10 µg/mL anti-NCL-Alexa®488 antibody, and incubated in ice for 45-60 min. As controls, untreated cells or cells incubated with IgG_{1k} isotype control, in PBS-BSA containing 16.7 µM of DSPE-PEG_{2k}-F3 micelles, were used. Cells were washed twice with PBS-BSA, resuspended in 400 µL of PBS-BSA and analyzed by flow cytometry in a BD FACScalibur system (BD Biosciences, USA). Non-viable cells were excluded using 7-aminoactinomycin D (7-AAD) (Sigma-Aldrich, USA) aiming at rule out the analysis of intracellular nucleolin.

Estimation of nucleolin cell surface density was performed by comparing the fluorescence values of Alexa488 in the FL1 channel with standard curves prepared with the Quantum™ MESF Alexa488-labeled microsphere kit as per manufacturer instructions. With this procedure, the number of Molecules of Equivalent Soluble Fluorochrome (MESF), a standardized measurement of fluorescence intensity, was calculated, using QuickCal v2.3 (Bangs Laboratories, USA). The cell Antibody Binding Capacity (ABC), i.e. the number of antibody molecules bound per cell was determined by the equation: ABC = MESF/7.46, where the denominator represents the fluorochrome/antibody ratio. Accordingly, assuming a 1:1 NCL:Antibody binding ratio, the ABC defined the cell surface NCL density per cell.

Intracellular doxorubicin delivery

For each cell line, 250,000 cells were incubated with PEGASEMP, at 0.4 or 0.8 mM of total lipid (in fully supplemented RPMI-1640 medium), for 1 h at 37°C. After washing with PBS, doxorubicin fluorescence was analyzed by flow cytometry.

Association and dissociation studies

The different cells lines were plated in 96-well plates at a density of 50,000 cells/well and allowed to adhere overnight. Cells were then incubated (from 15 min to 8 h) with serial dilutions of rhodamine-labeled F3-peptide targeted liposomes (ranging from 0.1 to 1.2 mM total lipid), at 4°C, to decrease energy-dependent processes thus preventing liposome internalization through endocytosis. As controls, liposomes functionalized with the non-specific peptide or plain liposomes (without ligand), and untreated cells [20, 26], were used as controls. Subsequently, cells were washed thrice with cold PBS. Cells were then lysed with 200 µl of lysis buffer (50 mM Tris-HCl, 150 mM NaCl, 0.1% (m/v) sodium lauryl sulfate, 5 mM EDTA and 1% (v/v) Triton-X100, pH 8.0) at 4°C. Rhodamine-PE fluorescence was measured in a SpectraMax Gemini EM plate reader fluorimeter (Molecular Devices, USA) at $\lambda_{excitation}$ 545 nm/$\lambda_{emission}$ 587 nm (λ_{cutoff} 570 nm). The amount of cell-associated lipid was drawn from rhodamine-PE calibration curves. Results were normalized against the total protein of each well, determined with the BCA™ Protein Assay Kit (Pierce, ThermoFisher Scientific, USA)

according to the manufacturer's protocol and using RIPA buffer to prepare the standards for the calibration curve.

Internalization studies

The kinetics of PEGASEMP internalization into cancer cells from diverse species was assessed by comparison with a non-targeted liposomal formulation of doxorubicin. Following the incubation of 50,000 cells with 0.4 mM of PEGASEMP (or control, from 0 to 1.5 h), at 37°C, cell surface-bound liposomes were removed with low pH buffer (40 mM citric acid, 120 mM NaCl pH 3.0). The total cell-associated doxorubicin and the internalized fraction were determined by measuring doxorubicin fluorescence in a SpectraMax Gemini EM plate reader fluorimeter (Molecular Devices, USA) at $\lambda_{excitation}$ 485 nm/$\lambda_{emission}$ 590 nm (λ_{cutoff} 570 nm).

Cytotoxicity evaluation

To evaluate cell viability, 4000 CMT3 cells, 8000 MDA-MB-435S and MDA-MB-231 cells, and 1500 4T1 cells, were incubated with serial dilutions of PEGASEMP-doxorubicin or non-targeted liposomes (0.2 to 50 μM), for 1, 4 or 24 h, at 37 °C in an atmosphere of 5% of CO_2, where recovery time with fresh medium lasted up to 95, 92 or 72 h, respectively. Subsequently, cell viability was evaluated using the resazurin reduction method. Briefly, cells were incubated with 10% of resazurin dye in culture medium at 37°C, for 2 h, followed by absorbance measurement at 540 nm (reduced form) and 630 nm (oxidized form) in a SpectraMax Gemini EM plate reader fluorimeter (Molecular Devices, USA). Cell viability was extrapolated from the resazurin reduction using the following expression: $[(\square_{oxi630} \times A_{540} - \square_{oxi540} \times A_{630})_{treated\ cells}/(\square_{oxi630} \times A_{540} - \square_{oxi540} - A_{630})_{untreated\ cells}] \times 100$.

Determination of nucleolin homology across species

Nucleolin amino acid sequences from different animal organs were obtained from Swiss-Prot (human, *Homo sapiens*, UniProtKB-P19338; mouse, *Mus musculus*, UniProtKB-P09405 and rat, *Rattus norvegicus*, UniProtKB-P13383) or TrEMBL protein database (canine, *Canis lupus familiaris*, UniProtKB-F1Q0B0) (http://www.uniprot.org/uniprot/) available from the Universal Protein Resource (http://www.uniprot.org/). With the exception of canine nucleolin (predicted by automated computational analysis of its genomic sequence) all other sequences were validated and reviewed by the Universal Protein Resource (http://www.uniprot.org/). Sequences were aligned using ClustalOmega version 1.2.1 (http://www.clustal.org/omega/) [28], publicly available in the EBI web server (The European Bioinformatics Institute, http://www.ebi.ac.uk/Tools/msa/clustalo/). Multiple alignment analysis was further complemented with Jalview v2.10.5 tool.

Modeling of the dynamics of F3 peptide-targeted nanoparticles

Kinetic model

The model, based on mass-action kinetics, is composed of three main components: nucleolin trafficking, multi-tether-based binding of F3 peptide-targeted liposomes, internalization, and cell death. The complete set of model reactions is shown in Supplementary Table 1 and parameters in Supplementary Table 2.

Nucleolin trafficking. At the cell surface, nucleolin is modeled as belonging to *sites* available for liposome occupation and binding U; the individual binding sites (individual nucleolin) are not modeled since it has been shown that ligand binding induces nucleolin clustering [29-31] including the F3 peptide [7]. This model assumes slow nucleolin diffusivity [32, 33], all the way down to essentially fixed nucleolin molecules in the presence of binding to a large multivalent ligand [34].

Liposome binding. Liposome L is introduced to the system via bulk solution. Given the size of the liposomes and the experimental conditions, the liposome settles to form a monolayer M on the cell surface [35, 36]. This is modeled as a first-order process with a characteristic time $1/k_{\text{settle}}$. Only a fraction f_{oncell} of monolayer liposomes are accessible to cell surface nucleolin binding sites. The presence of a liposome at a site occludes other liposomes from occupying and binding to nucleolin molecules at that site. Liposome-nucleolin binding is modeled by the formation/breaking of individual tether-nucleolin interactions. The formation of the first tether, indicating the transition to the first bound state B_1, is modeled as a second-order process, as monolayer liposomes find an unoccupied site. Subsequent individual tethers i form one at a time up to n total tethers according to a first-order intermolecular process [33, 37-39]. Tethers also break one at a time according to a first-order process. The model tracks bound liposome-nucleolin site complexes B_i as *per-macrostate*, where a macrostate is composed of the $\binom{n}{i}$ microstates with i bound tethers. Each microstate with i bound tethers has i ways of unbinding and n-i ways of binding. The macroscopic concentrations and rates are then calculated by summing the microscopic concentrations and rates. Each macrostate B_i thus has i ways of unbinding and n-i ways of binding. The total number of tethers n is determined during the parameter fitting process by checking model goodness-of-fit with different n, subject to an upper bound on accessible tethers calculated from the liposome formulation properties.

Liposome internalization. Each bound liposome-nucleolin state B_i is allowed to internalize according to the standard clathrin-dependent receptor-mediated endocytosis mechanism [40-42]. Although there are other internalization mechanisms, including fluid-phase endocytosis, the single mechanism was chosen because it is expected to be the predominant mechanism for nucleolin internalization and for

the studied liposome concentrations [33, 43-45]. As a simplification, all bound states endocytose according to a first-order process with the same rate [46].

The resulting endosome is represented by two species, the now-available internalized nucleolin E and liposome I_0. These two components partition into recycling and degradation fates according to rates k_{rec} and k_{deg}, respectively [33]. Nucleolin and liposome have different partitioning fractions, where f_{rdeg} and f_{ldeg} indicate the fraction with degradation fate. Degraded components are removed from the cell. Recycled components are returned to the cell surface as unbound states.

The internalized liposome also participates in a drug release fate which releases doxorubicin into the cell. Internalized doxorubicin is tracked *per-liposome* (i.e., the cell is exposed to x liposomes containing doxorubicin over time) as I_j. Doxorubicin remains in the cell according to a time delay represented by a sequence of m first-order reactions, and is then cleared from the cell. The appropriate m is determined from fitting the model to internalization data in a fashion similar to that of n above. The total internalized doxorubicin, $\sum_{j=0}^{m} I_j$, integrated over the experiment duration was used as a metric of total drug exposure to link to the high-level cell killing model. This metric has previously been used in studies of doxorubicin's tumor cell killing and cardiotoxicity modes of action [47, 48]. Intracellular trafficking and nuclear localization of doxorubicin is not explicitly modeled because spatially resolved intracellular doxorubicin levels were not measured.

In the absence or presence of liposome, cell surface nucleolin molecules participate in the production, endocytosis, recycling, and degradation mechanisms [33, 49]. Nucleolin sites are also tracked *per-liposome* (i.e., x liposome binding sites' to nucleolin are transited through the cellular dynamics). The initial unbound surface nucleolin site concentration for each cell line is determined by calculating the steady-state of just this subset of the model and has the form:

$$U_0 = \frac{k_{prod}[f_{rdeg}(k_{deg} - k_{rec}) + k_{rec}]}{f_{rdeg} k_{deg} k_{endo}} \qquad \textit{(Equation 1)}$$

The experiments were performed at two temperatures: low temperature (4ºC) for association and high temperature (37ºC) for internalization and cell killing. The mechanisms in the model exhibit temperature dependence, with higher temperatures giving faster rates in general [50]. This is modeled by adding a temperature scaling factor for the binding/unbinding on/off rates $T_{scale,b}$ and nucleolin dynamics $T_{scale,r}$ (Supplementary Table 2). No additional temperature scaling factor is included for the internalized liposome and doxorubicin dynamics because these reactions are assumed to take place at high temperature only [33, 51].

Cell death modeling

The cell death model consists of a Hill function that relates the total internalized drug exposure to percent cell death [52, 53]:

$$\%\ \text{Dead} = \frac{\text{AUC}^n}{\text{EC}_{50}^n + \text{AUC}^n} \quad \textit{(Equation 2)}$$

It is constrained so that zero exposure produces zero cell death and infinite exposure produces complete (100%) cell death. The two remaining parameters are the exposure that produces 50% cell death EC_{50} and the Hill exponent that controls the steepness of the transition n. The use of total exposure as the independent variable allows for comparison of a variety of dosing amounts and times.

Model implementation and fitting

Model parameter fitting was performed in two steps: (1) fit parameters for the nucleolin and liposomal dynamics model, and (2) fit parameters for the cell killing model. Model construction, fitting, simulation, and analysis were performed with Matlab 2017b (The MathWorks, Inc., Natick, MA).

The nucleolin and liposomal dynamics model were fit to association and internalization data from all cell lines tested, at multiple doses, simultaneously comprising 45 experimental conditions. Previous work by Waters *et al.* has employed such an overall parameter fitting procedure [54]. For each cell line, the association data consisted of surface-bound nucleolin concentration over time at five doses, and the internalization data consisted of surface-bound nucleolin and internalized liposome concentration over time at two doses each. All species concentrations were converted to count per cell units. Low-temperature association and high-temperature internalization modes were combined by augmenting the low-temperature experiments with scaling factors that take on values ≤1. The model parameters and scaling factors were fit simultaneously (Supplementary Table 2).

The parameters k_{prod}, k_{endo}, and k_{rendo} were free to have different values between the cell lines. The model allows these values to be cell line-specific based on putative differences in cellular activity.

The parameter k_{off} has different values between species. The model allowed the off-rate of the nucleolin-tether interaction to be species-specific based on differences between nucleolin structure between species according to the nucleolin homology analysis. The other parameters were shared between cell lines. The model treated initial cell surface nucleolin concentration according to the steady-state induced by the model reactions at zero liposome concentration Eq 1. The initial monolayer and cell surface bound liposome concentrations were fixed at zero for all simulated conditions, as are all internalized liposome and released product concentrations.

The model treated measurements of cell surface bound liposome as the sum of all bound species $\sum_{i=1}^{n} B_i$, i.e., not distinguishing between states of *i* bound tethers. Similarly, measurements of internalized liposome were compared to the sum of all released products inside the cell $\sum_{j=0}^{m} I_j$.

Model parameters were fit to data using generalized least squares according to the objective function:

$$\chi^2(\theta) = e^T(\theta)V_{\bar{y}}^{-1}e(\theta) \qquad \textit{(Equation 3)}$$

$$e(\theta) = \bar{y}(\theta) - \hat{y} \qquad \textit{(Equation 4)}$$

Where θ is the vector of *n* parameters, $V_{\bar{y}}^{-1}$ is the covariance matrix of the measurements and $e(\theta)$ is the difference between the model predictions $\bar{y}(\theta)$ and data points $\bar{y}(\theta)$. $V_{\bar{y}}^{-1}$ is a square symmetric positive semi-definite matrix of size $n_{\bar{y}}$ number of measurements, and $e(\theta)$, $\bar{y}(\theta)$, and $\hat{y}$ are vectors of length $n_{\bar{y}}$. In this problem, the measurements were assumed independent with diagonal variance values corresponding to the measured variance from the experimental replicates. For each parameter fitting problem, all assembled experiments were simulated and optimized simultaneously.

The best-fit parameters were defined as the vector θ that minimized $\chi^2(\theta)$. This nonlinear optimization was performed using the KroneckerBio toolbox developed in the Tidor Lab with extensions to support multi-subject simulation and optimization with hierarchical parameter dependence (https://github.com/kroneckerbio). Internally the Optimization Toolbox's fmincon was used to solve the constrained nonlinear optimization problem. Multistart fits -- optimizing Eq 3 multiple times with different starting parameter values θ_0 - were performed. The finished fit ensemble was examined and the best fit, along with all fits within 2% of the best fit's $\chi^2(\theta)$ (corresponding to visually similar traces) were maintained.

The cell killing model's two parameters were fit for each cell line separately. For each experimental condition of the cell killing assay (1, 4, and 24 h incubation at nine doses each for a total of 27 conditions), the nucleolin and liposomal dynamics model was run using that cell line's parameters to simulate the species concentrations over time. At the end of the initial incubation time, a wash step was simulated by adding dummy reactions that rapidly deplete the bulk *L* and monolayer *M* concentrations over 15 min. Then the total internalized doxorubicin $\sum_{j=0}^{m} I_j$was integrated until the 72 h time-point to get the total drug exposure AUC. Each such AUC was related to the measured percent cells killed from the cell killing assay according to Eq 2. The percent of cells killed in each assay condition was calculated by subtracting the percent cells alive from a control without drug from the percent cells alive from a trial at each assay condition, averaged over three replicates. The

optimization of the two parameters EC_{50} and n was performed using the Matlab Optimization Toolbox's nonlinear least-squares solver lsqnonlin.

Nucleolin density perturbation analysis

To examine the effect of cell surface nucleolin concentration on association, internalization, and cell killing, perturbation studies were performed. The steady-state cell surface nucleolin concentration was multiplied by a scaling factor ranging from 1/3 to 3, and a corresponding model output of interest was calculated. The calculation was repeated for every member of the good fit parameter ensemble and the overall range of model outputs was analyzed. For association, the output was the steady-state surface bound liposomal concentration in the absence and presence of endocytosis (k_{endo} set to zero), evaluated at a set liposomal concentration. For internalization, the output was the summed flux of all the endocytosis *reactions* evaluated at a set liposomal concentration. A liposomal concentration of 0.4 mM was used for both analyses. For cell killing, the output was the percentage of death cells at the end of a 72 h period given a set of liposomal dose and incubation period.

Results

Assessment of nucleolin conservation across species

Nucleolin is a multifunctional protein that has been identified and sequenced in different mammalian species, including mouse [55], rat [56] and human [57]. Thus, information on some of the physical features of nucleolin from different mammals (human, dog, rat, and mouse) was obtained from public protein databases (Table 1).

Table 1. Physical characteristics of nucleolin in diverse mammalian species.

UniProtKB Entry	Organism	No. of amino acids	Molecular weight (kDa)*	pI*	
P19338	*Homo sapiens* (Human)	710	76.61	4.60	[57]
F1Q0B0	*Canis familiaris* (Dog)	715	77.48*	4.58*	[58]**
P09405	*Mus musculus* (Mouse)	707	76.72	4.68	[55]
P13383	*Rattus norvegicus* (Rat)	713	77.15	4.46	[56]

*Molecular weight and theoretical isoelectric point computed from amino acid sequence (http://www.uniprot.org/uniprot/). **Reference to the article presenting a high-quality draft genome sequence of the domestic dog, enabling prediction of protein sequence.

Despite their different origins, nucleolin from these four mammalian species presented a similar macromolecular structure with a similar number of amino acids, molecular weight and isoelectric point (Table 1), indicating a high level of sequence conservation and physical-chemical amino acid properties. In fact, it has been shown that nucleolin extracted from human, hamster or mouse cells presented the same specificity and affinity towards a mouse RNA fragment, containing a nucleolin recognition motif [59]. Conservation of the primary structure was further confirmed by multiple sequence alignment of these four proteins (Figure 1a) and in line with the previously characterized structural analysis in human, rat and mouse [60, 61]), and biological function as well (for a review see [61-63]).

Nucleolin multifunctionality arises from the structural organization of four domains present in all sequences analyzed: the N-terminal domain composed of highly acidic regions interspersed with basic regions and several phosphorylation sites; a nuclear localization signaling domain (NLS); the central domain containing four RNA-binding domains (RBD); and the C-terminal domain (GAR domain), rich in glycine, arginine and phenylalanine residues (Figure 1b).

Comparative analysis of protein sequence indicates a relative identity above 84% between nucleolin from different species (Figure 1c). Among the sequences analyzed, the highest levels of homology were between rat and mouse (93%), and human and canine (93%) (Figure 1c,d). The mouse and rat nucleolin showed a level of homology with the human nucleolin of 84 and 85%, respectively (Figure 1c,d). Interestingly, most of the substitutions observed among the protein sequences in the different species were semi-conserved, as the corresponding amino acids preserved the physical-chemical properties of the original residue (e.g., polarity or acid/base properties, Figure 1d).

Overall, the high sequence conservation of nucleolin among these species may be reflective of similar structure and function [59]. Accordingly, the impact of the observed nucleolin homology was assessed in the context of the binding and internalization of F3 peptide-targeted pH-sensitive and pegylated liposomes.

Fig. 1 Multiple alignment of nucleolin amino acid sequences in different mammalian species. (a) Amino acid sequences were obtained from the Swiss-Prot and TrEMBL protein databases (Table 1). Sequences were aligned using Clustal Omega. (b) Schematic representation of nucleolin domains in mammals. Acid/basic region in green, nuclear localization signaling (NLS) region in purple, RNA-binding domains (RBD) in blue, and glycine-arginine rich (GAR) domain in orange. (c) Nucleolin relative identity (%) across species from multiple alignment. (d) Detailed amino acid alignment of nucleolin

across species. Consensus (given by yellow histogram or blue gradient background) was calculated from the multiple alignment. The different regions of nucleolin are marked using the color scheme from (b).

A single kinetic model to capture the dynamics of F3 peptide-targeted liposomes binding to cell surface nucleolin

After establishing nucleolin homology and conservation across species, a kinetic computational model was developed aiming at understanding the various steps underlying the dynamics of interaction between nucleolin and F3 peptide-targeted liposomes, upon fitting experimental kinetic data (Fig. 2a) from cells of different origins. The model consists of coupled ordinary differential equations modeling the concentrations of bulk liposomal suspensions, cell surface and intracellular nucleolin, and liposome component concentrations according to experimental settings (Supplemental Table 1). This treats the concentrations of species, including extracellular, bound, and internalized liposomes, and surface and internalized nucleolin, and others, as time-varying quantities that interconvert between each other via reactions with specified rates. These reactions can represent binding and unbinding, transport of species between physical compartments such as endocytosis and recycling, production and clearance of molecules, and other processes (Supplemental Table 1). The model was constructed on a per-cell basis, with concentrations indicating counts of species per cell considering compartments as *well-mixed*, ignoring spatial dependence (for example, species interact freely within a cell) except in transport between compartments.

Initially, a fraction of liposomes (L) settles as a monolayer (M) ($f_{oncell}k_{settle}$) (Fig. 2a). From this state, liposomes will occupy a nucleolin binding site (U), which prevents further liposome occupation and binding. Such modeling of nucleolin, instead of individual molecules, relied on the evidence that several nucleolin-binding ligands (such as midkine, pleiotrophin or HB-19) promote nucleolin clustering into membrane patch-like domains [29-31]. After U site occupation, the first tether is formed (as B_1 complex) in a second-order process (k_{on2}) (Fig. 2a). Subsequent tethers form one at a time (up to n total tethers) in a first-order intermolecular process (k_{on}) [33, 37-39]. Each complex B_i (liposome bound to nucleolin-binding site by i tethers) internalizes according to a mechanism based on clathrin-dependent endocytosis as a first-order process (k_{endo}) (Fig. 2a). The products of this process are represented by the now-available internalized nucleolin site (E) and liposome (I_0). The latter also enabled to track doxorubicin in a *per-liposome* basis (i.e., the cell is exposed to x liposomes containing doxorubicin over time) as I_j, under a time delayed sequence of m first-order reactions (k_{delay}), that finally end in its clearance from the cell (k_{clear}) (Fig. 2a). The model also accommodates both degradation and recycling of nucleolin ($f_{rdeg}k_{deg}$ and $(1-f_{rdeg})k_{rec}$) and liposomes ($f_{ldeg}k_{deg}$ and $(1-$

$f_{ldeg})k_{rec}$). The same model topology is used for all cell types, but cell-specific parameters required estimation.

The model informing and fitting was performed over data collected from *in vitro* kinetic experiments on F3 peptide-targeted liposomes fluorescently labeled with rhodamine or loaded with doxorubicin (the latter named PEGASEMP) with 4T1 (mouse), MDA-MB-231 (human), MDA-MB-435S (human) and CMT3 (canine) cancer cell lines (Supplementary Fig. 1). The human MDA-MB-435S cancer cell line was used as a positive control for nucleolin expression throughout experiments, as the initial characterization of nucleolin-binding F3 peptide was performed with it [17, 20]. In each case, the corresponding lipid or doxorubicin doses were converted to a nominal number of liposomes and further normalized to cell number (i.e., *x* liposomes containing doxorubicin *per* cell) according to the surface area method [64].

At 4°C, a temperature not permissive to endocytosis [26], the binding of F3 peptide-targeted rhodamine labeled liposomes to cell surface nucleolin reflected a saturation across the cell lines tested, at the different liposomal densities incubated, which was generally described by the model (Fig. 2b, Supplementary Fig. 2). Interestingly though, the level at which the saturation plateau was reached depended on the incubated liposome density, stabilizing at a value above 8.48×10^6 liposomes/cell (Fig. 2b). Nevertheless, the model predicted that the total surface bound liposome reached a plateau within 2 h, regardless the cell line or liposome density (Fig. 2b). At a temperature permissive to endocytosis (37°C), despite the underestimation provided by the model (Supplementary Fig. 3), binding is also a saturable mechanism (Fig. 2c). Yet, nucleolin still enables the continued cellular internalization of PEGASEMP (F3 peptide-targeted liposomes loaded with doxorubicin) at a biphasic rate: fast over the first 20 min and slower beyond, the latter matching binding saturation (Fig. 2b). In contrast, the non-targeted doxorubicin-loaded liposomes exhibited similar profiles for binding and internalization kinetics, reflecting a non-active and stochastic nature of their interaction (Fig. 2c).

Altogether, the modeling indicated that binding to nucleolin is both time and liposomal dose dependent, yet it is not a limitation on the continuous internalization of bound F3 peptide-targeted nanoparticles.

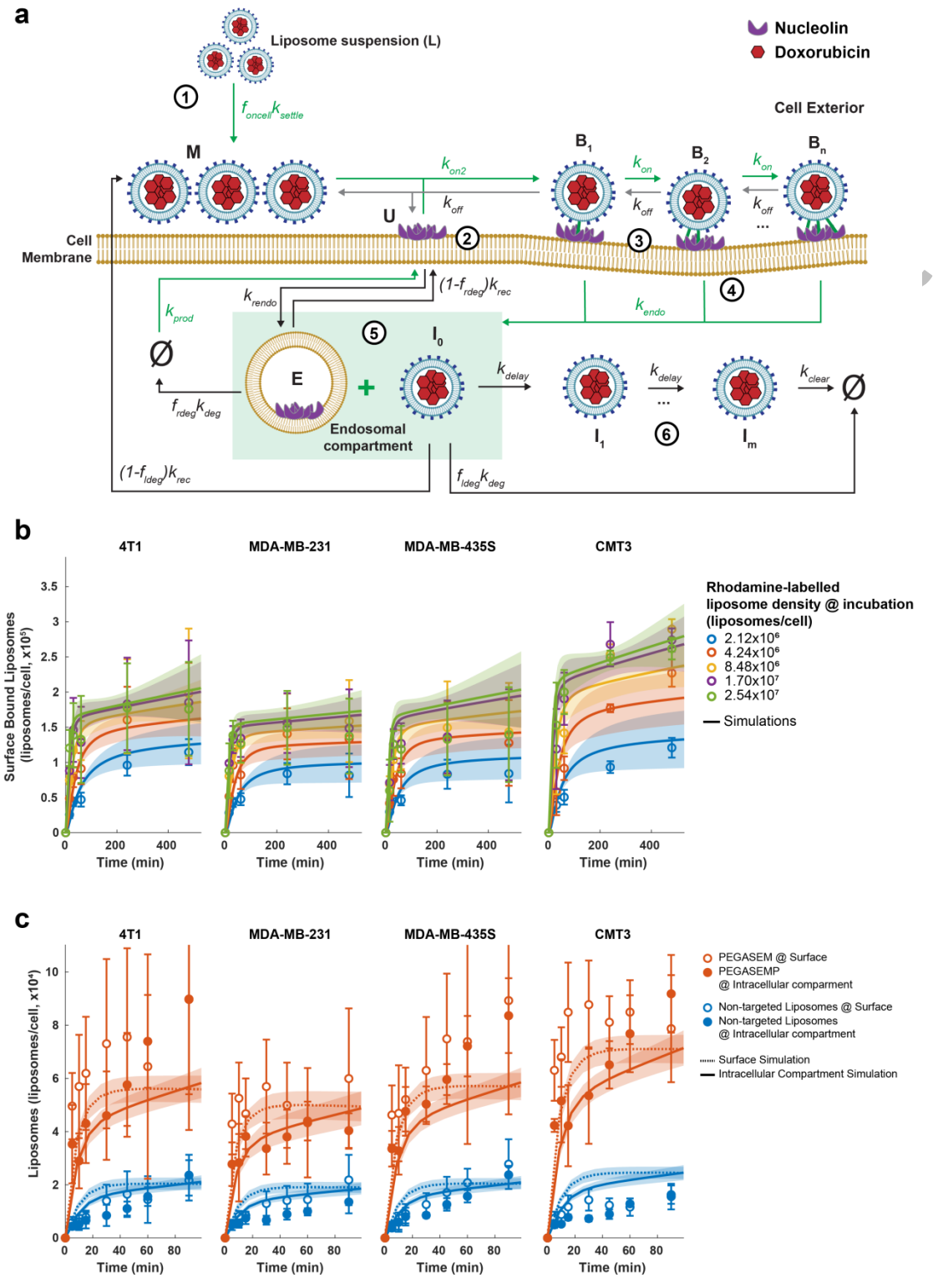

Fig. 2 Modeling binding and internalization of liposomes targeted by the nucleolin-binding F3 peptide. (a) The proposed multistep model for the binding and internalization of F3 peptide-targeted liposomes. 1) Liposomes (*L*), introduced in the system as bulk suspension, sediment (k_{settle}) to form a monolayer (M) on the cell surface. 2) Nucleolin is modeled as part of

binding sites (U) available for liposome occupation and binding, further occluding additional liposome binding onto the correspondent binding site. 3) The liposome-nucleolin binding is modeled as individual tether-nucleolin microstates forming a complex (B_i). 4) Each bound liposome-nucleolin site complex (B_i) is then internalized according the standard clathrin-dependent endocytosis mechanism as first-order process (k_{endo}). 5) The resulting endosome is represented by the now-available internalized nucleolin (E) and liposome (I_0), which undergoes recycling (k_{rec}) and degradation (k_{deg}). 6) The liposome I_m also enables the tracking of doxorubicin release fate on a per-liposome basis (i.e., cell is exposed to x liposomes containing doxorubicin) represented as m first-order reactions (k_{delay}), including cell clearance (k_{clear}). (b) Levels of surface-bound, rhodamine-labelled, F3 peptide-targeted liposome over time upon incubation with 4T1, MDA-MB-231, MDA-MB-435S and CMT3 cell lines at the indicated liposome densities at 4°C. (c) Surface-bound and internalized levels of PEGASEMP (orange) or non-targeted liposomes (blue) as a function of time after incubation with 4T1, MDA-MB-231, MDA-MB-435S and CMT3 cell lines with 8.48×10^6 liposomes/cell at 37°C. The symbols indicate the mean of experimental measured data ± SD (n=3). The ensemble's mean simulated liposome concentration over time is shown as the solid lines and SD as the shaded region.

Modeling the effect of the nucleolin/F3 peptide dynamics on doxorubicin exposure and cell death

After modeling the kinetic interaction of F3 peptide-targeted liposomes with cells expressing different molecular levels of surface nucleolin (Fig. 2), it was important to understand how this would translate into the actual cell exposure to delivered doxorubicin, and how in turn this would correlate with cancer cell death.

The model captured the biological mechanisms of nucleolin and F3 peptide-targeted liposome dynamics on the time scale of seconds to hours and was readily parameterized using the kinetic studies performed in this work (Fig. 2). However, cell killing behavior, which takes place on a time scale of hours to days, does not have detailed kinetic measurements, and thus is more readily captured by a coarser-grained model. Commonly, this pharmacodynamic effect is modeled by relating the area under the curve (AUC) of drug concentration from a pharmacokinetic model (in this case, the nucleolin and liposome dynamics model that yields the internalized doxorubicin concentration over time) to the cell death data [65]. The AUC constitutes an overall drug exposure metric calculated from an experimental condition. A simple expression, a Hill function, is then used to relate this drug exposure metric to cell killing [52].

According to the kinetic modeling of PEGASEMP binding and internalization (Fig. 2), the cell exposure to doxorubicin, mediated by PEGASEMP, at the different conditions used (incubation time and liposome dose), was modeled. It was reduced to a single dimension as the total doxorubicin exposure (AUC) (as x liposomes containing doxorubicin *per* cell at a given time), as a function of

liposome dose, following the conditions explored in the experimental determination of PEGASEMP's impact on cell death. For each cell line tested, the simulation demonstrated that the higher the liposome dose and the longer the incubation period, the larger the total doxorubicin exposure (Fig. 3a). In fact, the MDA-MB-231 cell line demonstrated the lowest exposure to doxorubicin, in contrast with CMT3 cells (Fig. 3a).

Such modeling enabled the prediction of nucleolin-mediated total doxorubicin exposure provided by the experimental settings of the assessment of PEGASEMP's impact on cell death, and thus extrapolation of global cell sensitivity to PEGASEMP. This approach actually differs from standard determination of effective cytotoxic concentrations, which normally reports values of incubation doses (from dose-response curves) rather than the actual intracellular bioactive drug exposures [66]. Accordingly, for each cell line tested, the measured cell death increased with total doxorubicin exposure (provided by liposomal dose and incubation time), as expected, and was accurately described by the Hill function [52] (equation 2, *Materials and Methods* section) (Fig. 3b). This enabled determination of important treatment sensitivity parameters, such as EC_{50} (effective doxorubicin exposure that enabled 50% cell death) and the Hill exponent *n* (curve steepness, hence sensitivity). In this respect, the 4T1 cell line was the most sensitive to PEGASEMP, as indicated by the higher *n*, as compared to the other cell lines (Fig. 3b). Furthermore, the EC_{50} among the cell lines tested spanned from 1.3 to 4.6 x 10^4 liposomes.cell^{-1}.h containing doxorubicin (Fig. 3b).

Altogether, a mean of $2.4x10^4 \pm 1.3x10^4$ liposomes.cell^{-1}.h containing doxorubicin eliciting 50% of cell death was determined from the modeling used, irrespective of cell sensitivity to doxorubicin.

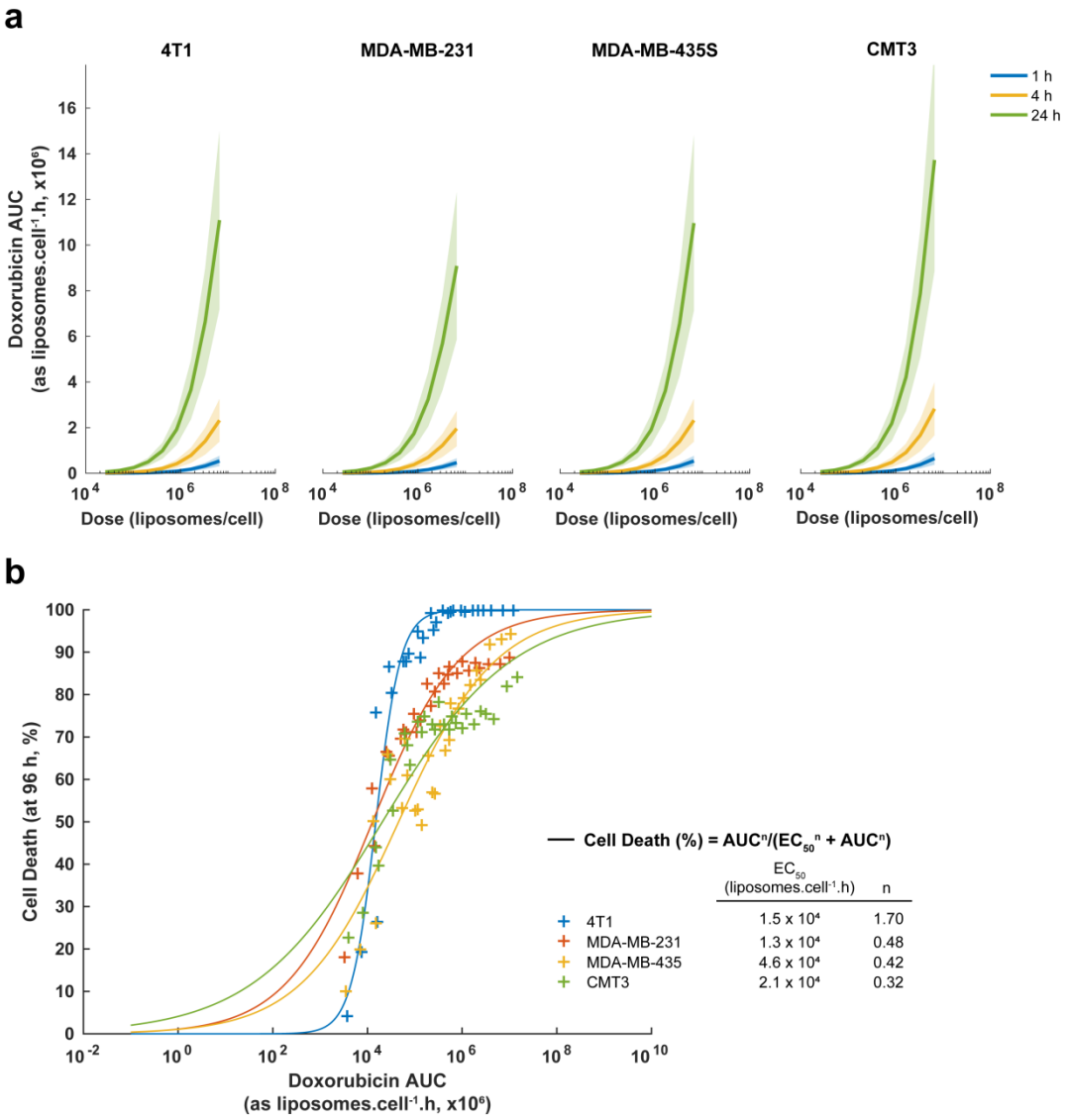

Fig. 3 Modulation of cell death as a function of doxorubicin exposure upon intracellular delivery by PEGASEMP. The indicated cell lines were incubated with PEGASEMP at serial dilutions, for 1, 4 and 24 h at 37°C, and then washed and allowed to recover in fresh medium for 95, 92 and 72 h, respectively. Doxorubicin content and cell death were evaluated. (a) Represents modeled total doxorubicin exposure (measured as number of liposomes per cell in an hour) upon cell incubation with PEGASEMP as a function of its dose (as liposomes/cell). Lines and shaded regions indicate mean and SD predictions, respectively. (b) Represents acquired (symbols, 27 condition combinations) and simulated (lines) cell death data as a function of doxorubicin exposure (AUC) provided from the different experimental settings for each cell line tested. The cell death model (Hill function) accounts the doxorubicin exposure (AUC) that enables 50% cell death (EC_{50}) and the Hill exponent (n) that defines function steepness.

Impact of the number of nucleolin-binding sites on *in vitro* biological outcomes of F3 peptide-mediated drug delivery

Establishing the impact of the level of expression of nucleolin-binding sites on the resulting pharmacodynamic interaction of the liposome with the target cell is critical, especially when tumors exhibit heterogeneity in such marker expression [24].

Accordingly, from the part of the model for PEGASEMP interaction with cell surface nucleolin, (Fig. 4a) plus parameters fit from above data, the probability density distribution for steady state surface nucleolin patch-like binding sites (U_0) was calculated according to Equation 1 (see *Materials and Methods* section) for each cell line. For 4T1, MDA-MB-231 and MDA-MB-435S cancer cells, nucleolin-binding sites ranged between 1.3 and 2.2 x 10^5 sites/cell, while 2.5 x 10^5 sites/cell were determined for CMT3 cells (Fig. 4b). These results, altogether, were in line with the determined trend on cell surface nucleolin density by flow cytometry (Fig. 4c) and liposome-interaction kinetics (Fig. 2).

To understand the impact of the number of nucleolin binding sites (U_0) on relevant output parameters, a perturbation analysis of U_0 was performed by multiplying nucleolin production rate k_{prod} by a scaling factor ranging from 1/3 to 3 and recording the resulting distribution of outputs (e.g., liposome bound to the surface). Under saturating conditions (413,897 liposomes/cell for 4 h), F3 peptide-targeted liposomes binding at the cell surface and total drug exposure mainly varied proportionally as a function of the variation of U_0 (Fig. 4d, e). Interestingly, the increase of surface bound liposome resulting from an increase in U_0 exhibited a smaller variation in the presence of endocytosis relative to its absence ($k_{rendo} = 0$) (Fig. 4d), a difference reflecting the spatial constraints of liposome binding in the absence of internalization.

A different perturbation behavior was observed for cell death. Under saturating exposures (413,897 liposomes/cell or 6,622,356 liposomes/cell for 4 or 24 h, respectively), U_0 variation had a minimal impact on cell death for the cell lines tested, as those conditions provided more than 85% of cell death (Fig. 4f and inserts). However, for non-saturating conditions of the internalization mechanism (25,869 liposomes/cell for 1 h; Fig. 2c), a 3-fold increase in U_0 enabled, approximately, 10% of cell death for cancer cells with similar sensitivity to doxorubicin (MDA-MB-231, MDA-MB-435S, and CMT3) (Fig. 4f). In the case of the 4T1 cancer cell line, no relevant variation was observed (Fig. 4f), reflecting its higher sensitivity to the delivered drug (Fig. 3b).

Overall, these data supported the notion that binding and internalization of liposomes functionalized with the F3 peptide, and subsequent cell exposure to doxorubicin-containing liposomes, increase

proportionally with nucleolin-binding sites. This pattern of variation is observed for the resulting cell death in non-saturating conditions, depending on the cancer cell sensitivity to doxorubicin.

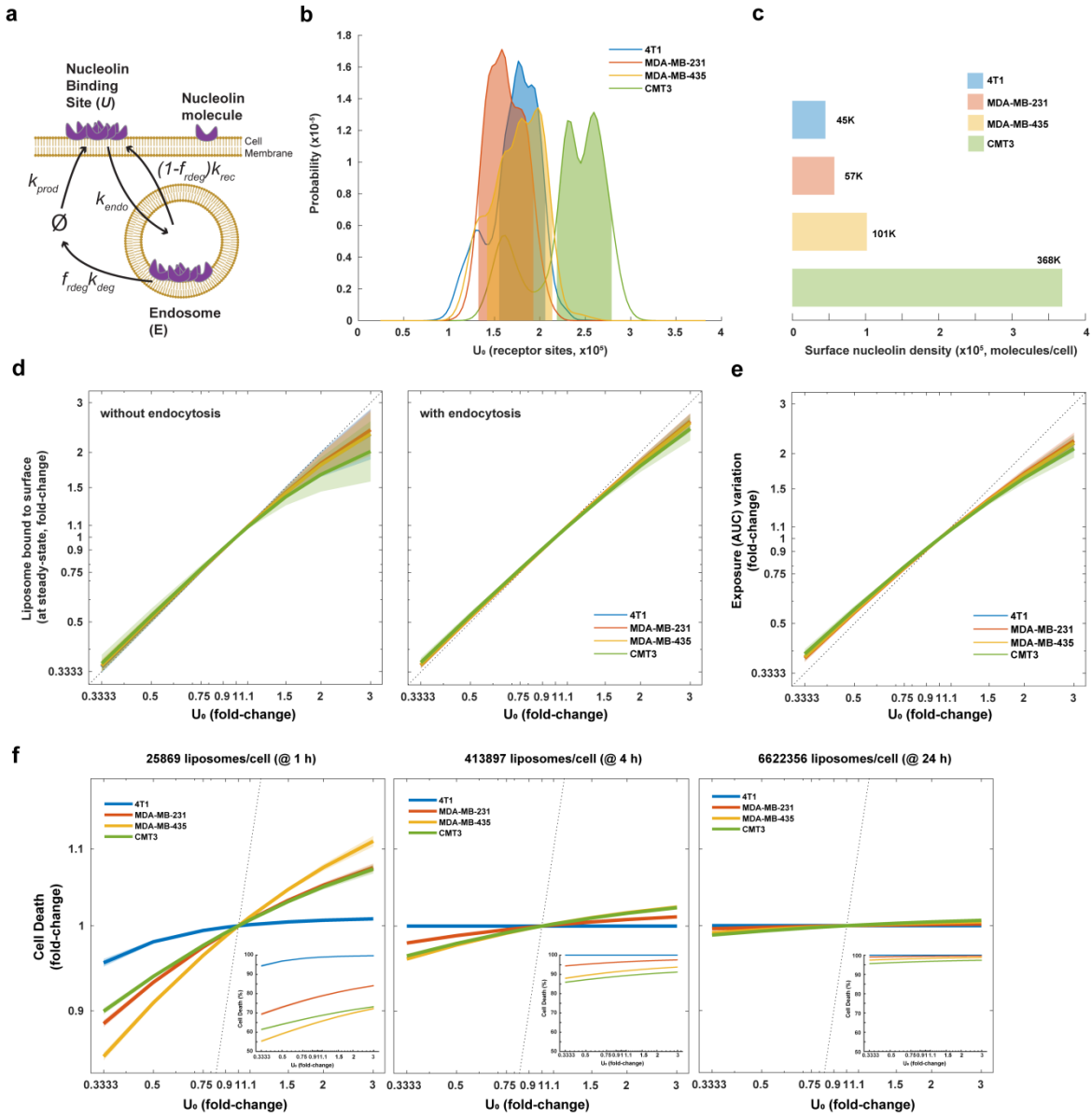

Fig. 4 Modulation of the impact of nucleolin-binding site density on critical parameters of liposomal interaction with cell lines from diverse species. (a) Diagram of the model behind steady-state nucleolin binding sites (*U*) at cell surface. In the absence or presence of F3 peptide-targeted liposomes, nucleolin is involved in the production (k_{prod}), endocytosis (k_{endo}), recycling ($(1-f_{rdeg})k_{rec}$), and degradation ($f_{rdeg}k_{deg}$) mechanisms of the binding sites (*U*). (b) Probability distribution of cell surface nucleolin binding sites at steady state (U_0) across cell lines from human and non-human origin calculated according to Equation 1 (see Materials and Methods). (c) Mean density of surface nucleolin per cell for the different cell lines (average values are shown near the bars). Determination of surface nucleolin levels by flow cytometry upon comparing the Alexa488 antibody-associated cell signal with calibrated bead standards; non-viable cells were excluded from analysis using 7-aminoactinomycin D. (d) Impact of the variation of nucleolin binding sites (*U*) on the steady state of surface bound-

liposomes targeted by the F3 peptide, either without (k_{endo} = 0) or with endocytosis, at a total lipid concentration of 0.2 mM (413,897 liposomes/cell) and 4 h incubation time. (e) Variation of doxorubicin exposure in response to change in nucleolin binding sites density (U_0), at a dose of 3.13 μM doxorubicin equivalent (413,897 liposomes/cell, or bulk 0.2 mM total lipid) and 4 h incubation time, at 37°C. (f) Represents the predicted impact of the variation of nucleolin binding sites density (U_0) on cell death, under low, medium and high exposure to PEGASEMP (25,869 liposomes/cell @ 1 h, 413,897 liposomes/cell @ 4 h and 6,622,356 liposomes/cell @24 h, respectively) at 37°C. Lines and shaded regions indicate ensemble mean and SD predictions, respectively. Dashed line represents the 1:1 variation.

Discussion

In the context of ligand-mediated drug delivery, an adequate characterization of the different features associated with a target receptor is one of the key issues for successful tumor targeting, and translation to patients [2, 3]. In particular, the identification of the differential expression profiles across tumor tissues, reflecting tumor heterogeneity, along with the assessment of targeting as a function of cellular dynamics and receptor levels is paramount to establishing such a target in an oncological setting [67] and efficiently designing a personalized, targeted delivery system [3]. Moreover, examining the target receptor homology across different animal species reinforces the validity of data collected across animal models of diverse species, helping translate the generated knowledge into patient benefit. Nucleolin has become a target for multiple therapeutic strategies, but still poorly explored in the clinical setting [6]. To understand how a novel liposomal pH-sensitive pegylated formulation functionalized with nucleolin-binding F3 peptide (PEGASEMP) interacts with cancer cells and how this translates to cell death, a combined *in vitro-in silico* kinetics study was performed. This was focused on the interactions across cancer cells from diverse species, thus guiding its translational development in the context of antitumor activity and non-specific toxicity across relevant species used throughout development [7].

The modeling work focused on the association and internalization of F3 peptide-targeted liposomes as a function of cell surface nucleolin (Fig. 2a) [26]. Uncertainty in model parameters was represented consistent with the experimental data (Supplementary Fig. 1 and Supplementary Table 2). To this end, nucleolin was modeled as a cluster of binding sites for the interaction with targeted liposomes instead of individual molecules. In fact, it has been described that several nucleolin-binding ligands (as midkine, pleiotrophin or HB-19) [29-31] promote nucleolin clustering into membrane patch-like domains, further supporting the modeling decision. Similarly, it had been previously demonstrated that binding of HER2-targeted liposomes and HER2 receptor was dependent on patch-like interactions [4]. Furthermore, the model was constructed under two assumptions regarding temperature dependence: (1) reaction rates are generally faster at higher temperature, and (2) no

endocytosis takes place at low temperature. These were handled by adding scaling factors that cause the low temperature rates to be some fraction lower than the high temperature rates. While those assumptions enabled good data fitting (Fig. 2), the model still provided, in some examples, over- and under-estimations compared to experimental results (Fig. 2b, c and Supplementary Fig. 2, 3). To refine the model in that aspect, adoption of physical-based values (i.e., interaction energies) and the introduction of a basal *leakage* endocytosis term, present at all temperatures, could be explored in future work.

Notwithstanding those constraints, the resulting ensemble of models was used to predict the range of possible system behaviors. In fact, the experimental kinetic behavior could be adequately explained by a single model for both liposome surface binding and internalization, using a minimum of cell line and species-specific parameters (Fig. 2b and 2c). Additionally, it enabled constructing a probability density function of the steady state nucleolin binding sites (U_0) for each cell line tested. The model demonstrated that the estimated U_0 sites, based on F3 peptide-targeted liposome/nucleolin interaction (Fig. 4b), correlated with surface nucleolin levels determined at the molecular level by flow cytometry (Fig. 4c). Yet, the model has some limitations in distinguishing finer differences compared to flow cytometry, owing to the multi-tether binding nature of liposomes to nucleolin, encompassed by the simulation. Nonetheless, the results were well aligned with the extent of surface-bound and internalized F3 peptide-targeted liposomes (Fig. 2b, c).

Importantly, modeling demonstrated that F3 peptide-targeted liposome binding to nucleolin did not limit their internalization (Fig. 2c). In fact, surface bound liposomes and exposure to doxorubicin increased proportionally with the number of nucleolin binding sites at steady state (U_0) (Fig. 4d, e). This observation was distinct from HER2-targeted liposomes, since their internalization was critically dependent on HER2 expression density at the cell surface, creating a threshold effect below which it was limited [4]. The difference may lay in the nature of both proteins and their dynamics. HER2 is a cell membrane receptor whose surface pool is slowly internalized (60-fold slower than clathrin-dependent transferrin) and dynamically mediated by caveolin-1 [68-70]. Nucleolin, on the other hand, does not present a transmembrane domain and its pathway of internalization, either clathrin-dependent or not, is dictated by the nature of the ligand [44, 71]. The nucleolin cell surface pool is further supported by its described nucleus-cytoplasm-membrane shuttling nature [18]. In fact, there is evidence that F3 peptide internalization by nucleolin relies on a clathrin-dependent pathway [45]. The mechanistically distinct surface dynamics between the two proteins may in part explain the threshold effect of HER2 on the internalization of HER2-targeted liposomes, under which multiple-low affinity interactions between the receptor and targeting moiety are essential to overcome HER2

membrane retention [4]. This membrane retention effect is apparently absent in the case of F3 peptide interaction with nucleolin, and the shuttling nature provides enough surface nucleolin molecules for continuous internalization in the different cell lines tested. Altogether, the data presented evidenced that nucleolin function, as an internalizing protein of F3 peptide-targeted liposomes, was conserved across species (Fig. 1).

Furthermore, it was possible to deduce, under a set of experimental conditions, the total doxorubicin exposure (as *x* doxorubicin-containing liposomes per cell and unit of time). This is a single dimension for every treatment condition representing the actual bioavailable and effective amount of the drug, which was further related to cell death using a Hill function model [52, 53] (Fig. 3). Yet, the individually estimated doxorubicin EC_{50} (Fig. 3b) did not automatically correlate with either the U_0 (Fig. 4b) values nor nucleolin surface density levels (Supplementary Fig. 4). Behind this observation is the fact that the different cell lines have different sensitivities to doxorubicin, regardless of nucleolin expression levels [27], intrinsically hindering such correlation. Nonetheless, it enabled one to estimate an effective *in vitro* exposure range that enables 50% of cell death across different cell sensitivities to doxorubicin and surface nucleolin levels – 1.1 to $3.7x10^4$ liposomes.cell^{-1}.h. Importantly, under lower exposures (within the estimated range), expected cell death varied proportionally with U_0 levels (except for 4T1 cells) (Fig. 4f). Solid tumors are heterogenous entities at the cellular level but also in the expression patterns of different markers, i.e. HER2, PSMA or even nucleolin, with manifest impact on treatment efficacy, and consequently on survival [24, 72-74]. Therefore, both predictions are of utmost value in the translation of such activity in the context of drug delivery to nucleolin-overexpressing solid tumors. If one accounts for the fact that estimated nanoparticle exposure in a solid tumor may fall within 1% of injected dose (intravenously), regardless its nature [75], proper characterization of tumoral nucleolin expression homogeneity will be paramount to successfully leveraging the activity provided by PEGASEMP. Anticipating that challenge, the data presented herein anticipates that flow cytometry could be explored to estimate steady state nucleolin levels (Fig. 4b, c), in line with similar methodologies for cell profiling [76].

Conclusion

Several nucleolin-targeting nanoparticles, based on ligands as aptamers or peptides, have been developed; however, the assessment of the relationship between nucleolin expression level and their pharmacodynamics, has been limited [77-79]. Accordingly, herein it was shown that nucleolin expression levels were not a limitation on the continuous internalization of F3 peptide-targeted liposomes, despite the saturable nature of the binding mechanism, and in line with previous observations on the fast nucleolin turnover from the cell surface [19]. Furthermore, under the

estimated mean EC_{50} (effective doxorubicin exposure that enables 50% cell death), it was shown that the activity may vary according to nucleolin expression. Such information becomes highly relevant when considering that nanoparticles, upon intravenous administration, reach tumors at a low percentage of injected dose and that tumors can be highly heterogenous in terms of antigen expression [18, 75]. This aspect significantly increases the importance of adequate tumor and patient characterization to extract the highest performance possible from ligand-mediated targeted strategies, and particularly the one herein studied. Importantly, in the context of development of nucleolin-based targeted drug delivery, the structural and functional similarities across species presented herein, emphasized the potential to use toxicological data and other metrics from lower species (e.g., dog; manuscript submitted for publication) to infer the dose for a first-in-human trial.

Ethical statement

Ethics approval and consent to participate:

Not applicable.

Consent for publication:

All authors agree with manuscript publication.

Availability of data and materials:

All data generated or analysed during this study are included in this published article [and its supplementary information files].

Competing interests:

V.M. and N.A.F. were former employees at TREAT U, SA. S.S., L.A. and J.N.M. are share-holders of TREAT U, SA. The remaining authors declare no competing interests.

Funding

This work was supported by the following projects: QREN/FEDER MultiNanoMed (Ref: 23240). This work was also financed by the European Regional Development Fund (ERDF), through the Centro 2020 Regional Operational Program under project CENTRO-01-0247-FEDER-017646 (ODD4PEGASEMP), and through the COMPETE 2020 - Operational Program for Competitiveness and Internationalisation and Portuguese national funds via FCT – Fundação para a Ciência e a Tecnologia, I.P., under projects POCI-01-0145-FEDER-016390 (CancelStem), Euronanomed (FCT reference ENMed/0005/2015), CENTRO-01-0145-FEDER-000012-HealthyAging2020 and CIBB (FCT reference UIDB/04539/2020).

Author's contributions:

R.L., K.S., and N.A.F. contributed equally for this work. R.L. designed and performed experiments, analyzed data, prepared figures, wrote and edited the manuscript. K.S. designed and performed the mathematical modeling, prepared figures, wrote and edited the manuscript. N.A.F. designed experiments, performed data interpretation, prepared figures, wrote, and edited the manuscript. A.G. provided support on the canine cell line and edited the manuscript. J.S.R. performed the conservation analysis and edited the manuscript. L.A. contributed to the design of the experiments. V.M. and S.S. supervised all the components of the study and edited the manuscript. B.T. supervised the mathematical modeling and edited the manuscript. J.N.M. supervised all components of this study, designed experiments, wrote and edited the manuscript.

Acknowledgements

MIT-Portugal Program.

References

1. Fonseca NA, Moura V, Colelli F, Pesce D, Cardile F, Pisano C, et al. Targeting nucleolin with doxorubicin-containing nanoparticle induces a significant tumor growth inhibition in an orthotopic animal model of standard of care-resistant mesothelioma. Cancer Research. 2017;77:5155-
2. Fonseca NA, Gregorio AC, Valerio-Fernandes A, Simoes S, Moreira JN. Bridging cancer biology and the patients' needs with nanotechnology-based approaches. Cancer Treat Rev. 2014;40:626-35
3. Srinivasarao M, Low PS. Ligand-Targeted Drug Delivery. Chem Rev. 2017;117:12133-64
4. Hendriks BS, Klinz SG, Reynolds JG, Espelin CW, Gaddy DF, Wickham TJ. Impact of tumor HER2/ERBB2 expression level on HER2-targeted liposomal doxorubicin-mediated drug delivery: multiple low-affinity interactions lead to a threshold effect. Mol Cancer Ther. 2013;12:1816-28
5. Munster P, Krop IE, LoRusso P, Ma C, Siegel BA, Shields AF, et al. Safety and pharmacokinetics of MM-302, a HER2-targeted antibody-liposomal doxorubicin conjugate, in patients with advanced HER2-positive breast cancer: a phase 1 dose-escalation study. Br J Cancer. 2018;119:1086-93
6. Gregorio AC, Lacerda M, Figueiredo P, Simoes S, Dias S, Moreira JN. Meeting the needs of breast cancer: A nucleolin's perspective. Crit Rev Oncol Hematol. 2018;125:89-101
7. Fonseca NA, Gregório AC, Mendes VM, Lopes R, Abreu T, Gonçalves N, et al. GMP-grade nanoparticle targeted to nucleolin downregulates tumor molecular signature, blocking growth and invasion, at low systemic exposure. Nano Today. 2021;37:
8. Srivastava M, Pollard HB. Molecular dissection of nucleolin's role in growth and cell proliferation: new insights. FASEB J. 1999;13:1911-22
9. Gaume X, Tassin AM, Ugrinova I, Mongelard F, Monier K, Bouvet P. Centrosomal nucleolin is required for microtubule network organization. Cell Cycle. 2015;14:902-19
10. Ugrinova I, Monier K, Ivaldi C, Thiry M, Storck S, Mongelard F, et al. Inactivation of nucleolin leads to nucleolar disruption, cell cycle arrest and defects in centrosome duplication. BMC Mol Biol. 2007;8:66
11. Xu JY, Lu S, Xu XY, Hu SL, Li B, Li WX, et al. Prognostic significance of nuclear or cytoplasmic nucleolin expression in human non-small cell lung cancer and its relationship with

DNA-PKcs. Tumour biology : the journal of the International Society for Oncodevelopmental Biology and Medicine. 2016;37:10349-56
12. Jain N, Zhu H, Khashab T, Ye Q, George B, Mathur R, et al. Targeting nucleolin for better survival in diffuse large B-cell lymphoma. Leukemia. 2018;32:663-74
13. Qiu W, Zhou F, Zhang Q, Sun X, Shi X, Liang Y, et al. Overexpression of nucleolin and different expression sites both related to the prognosis of gastric cancer. APMIS. 2013;121:919-25
14. Chen C, Chen L, Yao Y, Qin Z, Chen H. Nucleolin overexpression is associated with an unfavorable outcome for ependymoma: a multifactorial analysis of 176 patients. J Neurooncol. 2016;127:43-52
15. Marcel V, Catez F, Berger CM, Perrial E, Plesa A, Thomas X, et al. Expression Profiling of Ribosome Biogenesis Factors Reveals Nucleolin as a Novel Potential Marker to Predict Outcome in AML Patients. PLoS One. 2017;12:e0170160
16. Berger CM, Gaume X, Bouvet P. The roles of nucleolin subcellular localization in cancer. Biochimie. 2015;113:78-85
17. Christian S, Pilch J, Akerman ME, Porkka K, Laakkonen P, Ruoslahti E. Nucleolin expressed at the cell surface is a marker of endothelial cells in angiogenic blood vessels. J Cell Biol. 2003;163:871-8
18. Fonseca NA, Cruz AF, Moura V, Simoes S, Moreira JN. The cancer stem cell phenotype as a determinant factor of the heterotypic nature of breast tumors. Crit Rev Oncol Hematol. 2017;113:111-21
19. Hovanessian AG, Soundaramourty C, Khoury DE, Nondier I, Svab J, Krust B. Surface expressed nucleolin is constantly induced in tumor cells to mediate calcium-dependent ligand internalization. PLoS One. 2010;5:e15787
20. Porkka K, Laakkonen P, Hoffman JA, Bernasconi M, Ruoslahti E. A fragment of the HMGN2 protein homes to the nuclei of tumor cells and tumor endothelial cells in vivo. Proc Natl Acad Sci U S A. 2002;99:7444-9
21. Lauffenburger DA, Linderman J, Berkowitz L. Analysis of mammalian cell growth factor receptor dynamics. Ann N Y Acad Sci. 1987;506:147-62
22. Rae JM, Creighton CJ, Meck JM, Haddad BR, Johnson MD. MDA-MB-435 cells are derived from M14 melanoma cells--a loss for breast cancer, but a boon for melanoma research. Breast Cancer Res Treat. 2007;104:13-9
23. Sellappan S, Grijalva R, Zhou X, Yang W, Eli MB, Mills GB, et al. Lineage infidelity of MDA-MB-435 cells: expression of melanocyte proteins in a breast cancer cell line. Cancer Res. 2004;64:3479-85
24. Fonseca NA, Rodrigues AS, Rodrigues-Santos P, Alves V, Gregorio AC, Valerio-Fernandes A, et al. Nucleolin overexpression in breast cancer cell sub-populations with different stem-like phenotype enables targeted intracellular delivery of synergistic drug combination. Biomaterials. 2015;69:76-88
25. Xiong Q, Wilson WK, Pang J. The Liebermann-Burchard reaction: sulfonation, desaturation, and rearrangment of cholesterol in acid. Lipids. 2007;42:87-96
26. Moura V, Lacerda M, Figueiredo P, Corvo ML, Cruz ME, Soares R, et al. Targeted and intracellular triggered delivery of therapeutics to cancer cells and the tumor microenvironment: impact on the treatment of breast cancer. Breast Cancer Res Treat. 2012;133:61-73
27. Fonseca NA, Gomes-da-Silva LC, Moura V, Simoes S, Moreira JN. Simultaneous active intracellular delivery of doxorubicin and C6-ceramide shifts the additive/antagonistic drug interaction of non-encapsulated combination. J Control Release. 2014;196:122-31
28. Sievers F, Wilm A, Dineen D, Gibson TJ, Karplus K, Li W, et al. Fast, scalable generation of high-quality protein multiple sequence alignments using Clustal Omega. Mol Syst Biol. 2011;7:539
29. Said EA, Courty J, Svab J, Delbe J, Krust B, Hovanessian AG. Pleiotrophin inhibits HIV infection by binding the cell surface-expressed nucleolin. The FEBS journal. 2005;272:4646-59

30. Said EA, Krust B, Nisole S, Svab J, Briand JP, Hovanessian AG. The anti-HIV cytokine midkine binds the cell surface-expressed nucleolin as a low affinity receptor. J Biol Chem. 2002;277:37492-502
31. Nisole S, Krust B, Hovanessian AG. Anchorage of HIV on permissive cells leads to coaggregation of viral particles with surface nucleolin at membrane raft microdomains. Exp Cell Res. 2002;276:155-73
32. Cherry RJ, Smith PR, Morrison IEG, Fernandez N. Mobility of cell surface receptors: a re-evaluation. FEBS Letters. 1998;430:88-91
33. Lauffenburger DA, Linderman JJ. Receptors. Models for binding, trafficking, and signalling. The International Journal of Biochemistry & Cell Biology. 1996;28:
34. Thoumine O, Saint-Michel E, Dequidt C, Falk J, Rudge R, Galli T, et al. Weak effect of membrane diffusion on the rate of receptor accumulation at adhesive contacts. Biophys J. 2005;89:L40-2
35. Laouini A, Jaafar-Maalej C, Limayem-Blouza I, Sfar S, Charcosset C, Fessi H. Preparation, Characterization and Applications of Liposomes: State of the Art. Journal of Colloid Science and Biotechnology. 2012;1:147-68
36. Bulbake U, Doppalapudi S, Kommineni N, Khan W. Liposomal Formulations in Clinical Use: An Updated Review. Pharmaceutics. 2017;9:
37. Perelson AS. Receptor clustering on a cell surface. III. theory of receptor cross-linking by multivalent ligands: description by ligand states. Mathematical Biosciences. 1981;53:1-39
38. Nir S, Peled R, Lee K-D. Analysis of particle uptake by cells: Binding to several receptors, equilibration time, endocytosis. Colloids and Surfaces A: Physicochemical and Engineering Aspects. 1994;89:45-57
39. Xu H, Shaw DE. A Simple Model of Multivalent Adhesion and Its Application to Influenza Infection. Biophys J. 2016;110:218-33
40. Straubinger RM, Hong K, Friend DS, Papahadjopoulos D. Endocytosis of liposomes and intracellular fate of encapsulated molecules: Encounter with a low pH compartment after internalization in coated vesicles. Cell. 1983;32:1069-79
41. Daleke DL, Hong K, Papahadjopoulos D. Endocytosis of liposomes by macrophages: binding, acidification and leakage of liposomes monitored by a new fluorescence assay. Biochimica et Biophysica Acta (BBA) - Biomembranes. 1990;1024:352-66
42. Düzgüneş N, Nir S. Mechanisms and kinetics of liposome–cell interactions. Adv Drug Deliver Rev. 1999;40:3-18
43. Bareford LM, Swaan PW. Endocytic mechanisms for targeted drug delivery. Adv Drug Deliv Rev. 2007;59:748-58
44. Zhu J, Miao Q, Tang J, Wang X, Dong D, Liu T, et al. Nucleolin mediates the internalization of rabbit hemorrhagic disease virus through clathrin-dependent endocytosis. PLoS Pathog. 2018;14:e1007383
45. Caldeira De Moura VLDN, De Almeida Moreira JNS, De Magalhaes SSP, Pedroso De Lima MDCM, inventorsTargeted delivery to human diseases and disorders. PT2012.
46. Birtwistle MR, Kholodenko BN. Endocytosis and signalling: a meeting with mathematics. Mol Oncol. 2009;3:308-20
47. Thorn CF, Oshiro C, Marsh S, Hernandez-Boussard T, McLeod H, Klein TE, et al. Doxorubicin pathways: pharmacodynamics and adverse effects. Pharmacogenet Genomics. 2011;21:440-6
48. Šimůnek T, Štěrba M, Popelová O, Adamcová M, Hrdina R, Geršl V. Anthracycline-induced cardiotoxicity: Overview of studies examining the roles of oxidative stress and free cellular iron. Pharmacological Reports. 2009;61:154-71
49. Brown MS, Anderson RGW, Goldstein JL. Recycling receptors: The round-trip itinerary of migrant membrane proteins. Cell. 1983;32:663-7

50. Moehren G, Markevich N, Demin O, Kiyatkin A, Goryanin I, Hoek JB, et al. Temperature dependence of the epidermal growth factor receptor signaling network can be accounted for by a kinetic model. Biochemistry. 2002;41:306-20
51. Tomoda H, Kishimoto Y, Lee YC. Temperature effect on endocytosis and exocytosis by rabbit alveolar macrophages. J Biol Chem. 1989;264:15445-50
52. Goutelle S, Maurin M, Rougier F, Barbaut X, Bourguignon L, Ducher M, et al. The Hill equation: a review of its capabilities in pharmacological modelling. Fundam Clin Pharmacol. 2008;22:633-48
53. Eliaz RE, Nir S, Marty C, Szoka FC, Jr. Determination and modeling of kinetics of cancer cell killing by doxorubicin and doxorubicin encapsulated in targeted liposomes. Cancer Res. 2004;64:711-8
54. Waters CM, Oberg KC, Carpenter G, Overholser KA. Rate constants for binding, dissociation, and internalization of EGF: effect of receptor occupancy and ligand concentration. Biochemistry. 1990;29:3563-9
55. Bourbon H-M, Lapeyre B, Amalric F. Structure of the mouse nucleolin gene. Journal of molecular biology. 1988;200:627-38
56. Bourbon H-M, Amalric F. Nucleolin gene organization in rodents: highly conserved sequenced within three of the 13 introns. Gene. 1990;88:187-96
57. Srivastava M, Fleming PJ, Pollard HB, Burns AL. Cloning and sequencing of the human nucleolin cDNA. FEBS Letters. 1989;250:99-105
58. Lindblad-Toh K, Wade CM, Mikkelsen TS, Karlsson EK, Jaffe DB, Kamal M, et al. Genome sequence, comparative analysis and haplotype structure of the domestic dog. Nature. 2005;438:803-19
59. Serin G, Joseph G, Faucher C, Ghisolfi L, Bouche G, Amalric F, et al. Localization of nucleolin binding sites on human and mouse pre-ribosomal RNA. Biochimie. 1996;78:530-8
60. González-Camacho F, Medina FJ. Nucleolins from different model organisms have conserved sequences reflecting the conservation of key cellular functions through evolution. Journal of Applied Biomedicine. 2004;2:151-61
61. Ginisty H, Sicard H, Roger B, Bouvet P. Structure and functions of nucleolin. J Cell Sci. 1999;112 (Pt 6):761-72
62. Mongelard F, Bouvet P. Nucleolin: a multiFACeTed protein. Trends Cell Biol. 2007;17:80-6
63. Tajrishi MM, Tuteja R, Tuteja N. Nucleolin: The most abundant multifunctional phosphoprotein of nucleolus. Commun Integr Biol. 2011;4:267-75
64. Epstein H, Afergan E, Moise T, Richter Y, Rudich Y, Golomb G. Number-concentration of nanoparticles in liposomal and polymeric multiparticulate preparations: empirical and calculation methods. Biomaterials. 2006;27:651-9
65. Gianni L, Vigano L, Locatelli A, Capri G, Giani A, Tarenzi E, et al. Human pharmacokinetic characterization and in vitro study of the interaction between doxorubicin and paclitaxel in patients with breast cancer. J Clin Oncol. 1997;15:1906-15
66. Pinto AC, Moreira JN, Simoes S. Ciprofloxacin sensitizes hormone-refractory prostate cancer cell lines to doxorubicin and docetaxel treatment on a schedule-dependent manner. Cancer Chemother Pharmacol. 2009;64:445-54
67. Peer D, Karp JM, Hong S, Farokhzad OC, Margalit R, Langer R. Nanocarriers as an emerging platform for cancer therapy. Nat Nanotechnol. 2007;2:751-60
68. Pereira PMR, Sharma SK, Carter LM, Edwards KJ, Pourat J, Ragupathi A, et al. Caveolin-1 mediates cellular distribution of HER2 and affects trastuzumab binding and therapeutic efficacy. Nature communications. 2018;9:5137
69. Leahy DJ. Structure and function of the epidermal growth factor (EGF/ErbB) family of receptors. Adv Protein Chem. 2004;68:1-27

70. Austin CD, De Maziere AM, Pisacane PI, van Dijk SM, Eigenbrot C, Sliwkowski MX, et al. Endocytosis and sorting of ErbB2 and the site of action of cancer therapeutics trastuzumab and geldanamycin. Mol Biol Cell. 2004;15:5268-82
71. Chen X, Kube DM, Cooper MJ, Davis PB. Cell surface nucleolin serves as receptor for DNA nanoparticles composed of pegylated polylysine and DNA. Mol Ther. 2008;16:333-42
72. Hanahan D, Weinberg RA. Hallmarks of cancer: the next generation. Cell. 2011;144:646-74
73. Rye IH, Trinh A, Saetersdal AB, Nebdal D, Lingjaerde OC, Almendro V, et al. Intratumor heterogeneity defines treatment-resistant HER2+ breast tumors. Mol Oncol. 2018;12:1838-55
74. Paschalis A, Sheehan B, Riisnaes R, Rodrigues DN, Gurel B, Bertan C, et al. Prostate-specific Membrane Antigen Heterogeneity and DNA Repair Defects in Prostate Cancer. Eur Urol. 2019;76:469-78
75. Wilhelm S, Tavares AJ, Dai Q, Ohta S, Audet J, Dvorak HF, et al. Analysis of nanoparticle delivery to tumours. Nature Reviews Materials. 2016;1:16014
76. Gedye CA, Hussain A, Paterson J, Smrke A, Saini H, Sirskyj D, et al. Cell surface profiling using high-throughput flow cytometry: a platform for biomarker discovery and analysis of cellular heterogeneity. PLoS One. 2014;9:e105602
77. Bates PJ, Reyes-Reyes EM, Malik MT, Murphy EM, O'Toole MG, Trent JO. G-quadruplex oligonucleotide AS1411 as a cancer-targeting agent: Uses and mechanisms. Biochimica et Biophysica Acta (BBA) - General Subjects. 2017;1861:1414-28
78. Hu Q, Gu G, Liu Z, Jiang M, Kang T, Miao D, et al. F3 peptide-functionalized PEG-PLA nanoparticles co-administrated with tLyp-1 peptide for anti-glioma drug delivery. Biomaterials. 2013;34:1135-45
79. Winer I, Wang S, Lee YE, Fan W, Gong Y, Burgos-Ojeda D, et al. F3-targeted cisplatin-hydrogel nanoparticles as an effective therapeutic that targets both murine and human ovarian tumor endothelial cells in vivo. Cancer Res. 2010;70:8674-83